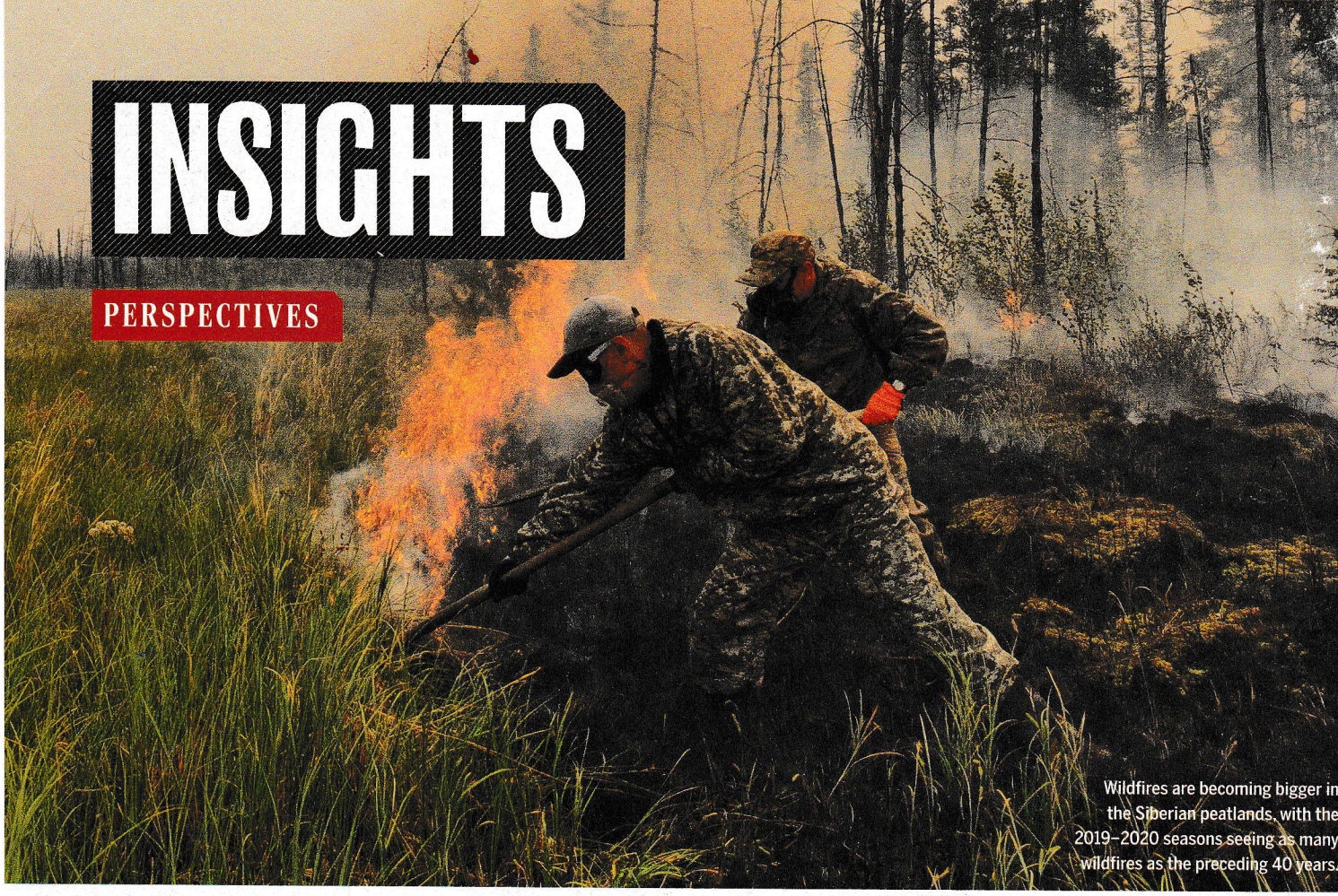

Wildfires are becoming bigger in the Siberian peatlands, with the 2019–2020 seasons seeing as many wildfires as the preceding 40 years.

CLIMATE CHANGE

Arctic wildfires at a warming threshold

Bigger wildfires in the Siberian Arctic signal release of more carbon to the atmosphere

By **Eric Post**[1] *and* **Michelle C. Mack**[2]

Vast amounts of organic carbon are stored in Arctic soils. Much of this is in the form of peat, a layer of decomposing plant matter. Arctic wildfires release this carbon to the atmosphere as carbon dioxide (CO_2) (*1*) and contribute to global warming. This creates a feedback loop in which accelerated Arctic warming (*2*) dries peatland soils, which increases the likelihood of bigger, more frequent wildfires in the Arctic and releases more CO_2, which further contributes to warming. Although this feedback mechanism is qualitatively understood, there remain uncertainties about its details. On page 532 of this issue, Descals *et al.* (*3*) analyze data from the 2019 and 2020 wildfire seasons in the Siberian Arctic and predict the extent of carbon-rich soils likely to burn in the area with future warming. Critically, they suggest that even minor increases in temperature above certain thresholds may promote increasingly larger wildfires.

Assessment of the relationship between climate warming and the frequency and extent of Arctic wildfires is complicated by several factors. Satellite data of the annual area burned by wildfires in the Arctic may require difficult-to-obtain ground-based validation to improve accuracy. Moreover, multiple factors may interact with warming in complex ways to influence fire occurrence, severity, and extent, such as lightning strikes, rainfall, and fuel load or vegetation cover. Add to this mix the uncertainty that derives from gaps in the geographic representation of data across the Arctic and the challenges seem almost insurmountable. The Siberian Arctic, for example, represents as much as 70% of the terrestrial Arctic, but year-to-year records of its burned area are sparse.

Descals *et al.* compiled multiple satellite-based estimates of the annual burned area for the Siberian Arctic from 1982 to 2020 to analyze associations between burned area and several factors (see the figure). According to their analysis across all sources of satellite data, 2019 and 2020 emerge as the biggest fire years for the Siberian Arctic, accounting for nearly half of the area burned for that region over the entire 39-year period and releasing nearly 150 million tonnes of carbon to the atmosphere. On 20 June 2020, the Russian town of Verkhoyansk set the record for the highest single-day temperature measured above the Arctic Circle (38°C) (*4*). On average, the Arctic region has warmed faster than the rest of the globe. Northern peatlands—including those in Asia, North America, and Europe—currently account for an annual carbon sink of ~100 million tonnes (*5*). The enormous carbon release of 150 million tonnes from the 2019 and 2020 Siberian

[1]Department of Wildlife, Fish, and Conservation Biology, University of California, Davis, Davis, CA, USA. [2]Center for Ecosystem Science and Society and Department of Biological Sciences, Northern Arizona University, Flagstaff, AZ, USA. Email: post@ucdavis.edu

fires demonstrates how quickly northern ecosystems can switch from carbon sinks to carbon sources under the continuous warming of the Arctic.

The authors started with individual single-predictor models, which mostly show exponential increases in burnt area across the Siberian Arctic for each of the individual drivers. These include the increases in temperature, vapor-pressure deficit (the ability of the air to dry the land surface), climatic water deficit (more water being evaporated relative to precipitation), and the number of ignition events presumably related to lightning strikes. Building on the single-predictor models, the authors then created a multivariate model, which revealed that some of the single-predictor drivers can themselves be driven by an increase in temperature. For example, warming can directly increase the number of ignition events and indirectly increase plant water stress by increasing the vapor-pressure deficit. This in turn can dry deeper soil layers and contribute to plant water stress. By linking these processes and identifying the direct and indirect effects of warming on increasing burn area, Descals *et al.* provide insights into what the future of Arctic wildfires may look like under accelerating warming.

According to their analysis, warming of mean summer air temperature past a threshold of 10°C, or of mean summer surface temperature above 17°C, would cause disproportionately large increases in the extent of carbon-rich soils burned in the Siberian Arctic. However, patterns of both local warming (*2*) and vegetation change (*6*, *7*) are highly variable across the Arctic. Therefore, additional studies in other regions of the Arctic that harbor vast expanses of peatland, such as Canada and Alaska (*5*), are needed to test these hypotheses and their general applicability to the Arctic region.

It is worth considering the implications of increasingly frequent and large wildfires for the fate of carbon that is currently locked away in the permafrost soils and sediments that underlie much of the Arctic. Increased combustion of the insulating peat layer can expose more permafrost and lead to the thaw and decomposition of an even larger reservoir of organic matter, releasing carbon that has been stored underground for centuries or even millennia (*8*). Larger and more intense wildfires could substantially accelerate the release of permafrost carbon into the atmosphere (*9*), but this interaction is not considered in current forecasts of Arctic feedback to global warming (*10*). Future studies that link rigorous assessment of wildfires with the dynamics of permafrost thaw in these remote regions are therefore needed to better quantify their impact on climate. ■

REFERENCES AND NOTES

1. M. C. Mack *et al.*, *Nature* **475**, 489 (2011).
2. M. Rantanen *et al.*, *Commun. Earth Environ.* **3**, 168 (2022).
3. A. Descals *et al.*, *Science* **378**, 532 (2022).
4. M. Allen, *Eos* **102** (2021).
5. G. Hugelius *et al.*, *Proc. Natl. Acad. Sci. U.S.A.* **117**, 20438 (2020).
6. C. G. Collins *et al.*, *Nat. Commun.* **12**, 3442 (2021).
7. I. Myers-Smith *et al.*, *Nat. Clim. Chang.* **10**, 106 (2020).
8. E. A. G. Schuur *et al.*, *Nature* **520**, 171 (2015).
9. S. M. Natali *et al.*, *Proc. Natl. Acad. Sci. U.S.A.* **118**, e2100163118 (2021).
10. Intergovernmental Panel on Climate Change, *Climate Change 2021: The Physical Science Basis. Contribution of Working Group I to the Sixth Assessment Report of the Intergovernmental Panel on Climate Change* (Cambridge Univ. Press, 2021).

ACKNOWLEDGMENTS

The authors thank P. F. Sullivan for comments on the manuscript.

10.1126/science.ade9583

The effect of Arctic wildfires on carbon release

Arctic wildfires accelerate the release of organic carbon from the soil into the atmosphere, which can strengthen the feedback to warming.

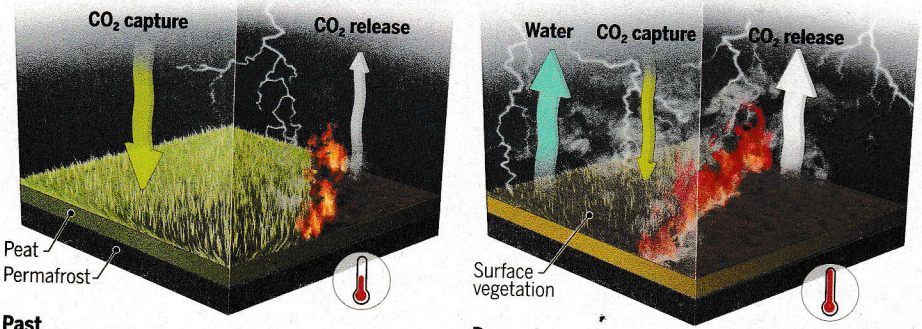

GRAPHIC: V. ALTOUNIAN/*SCIENCE*

Past
Arctic peatlands, forests, and tundra are generally carbon sinks. Cold temperatures and wet soils keep the land relatively moist, which reduces wildfire activity

Present
Higher temperatures dry the peat layer and drive more active weather systems, which lead to more frequent lightning strikes, creating larger fires that release more carbon to the atmosphere.

ARCTIC WILDFIRES

Unprecedented fire activity above the Arctic Circle linked to rising temperatures

Adrià Descals[1,2]*, David L. A. Gaveau[3], Aleixandre Verger[1,2,4], Douglas Sheil[5,6], Daisuke Naito[6,7], Josep Peñuelas[1,2]

Arctic fires can release large amounts of carbon from permafrost peatlands. Satellite observations reveal that fires burned ~4.7 million hectares in 2019 and 2020, accounting for 44% of the total burned area in the Siberian Arctic for the entire 1982–2020 period. The summer of 2020 was the warmest in four decades, with fires burning an unprecedentedly large area of carbon-rich soils. We show that factors of fire associated with temperature have increased in recent decades and identified a near-exponential relationship between these factors and annual burned area. Large fires in the Arctic are likely to recur with climatic warming before mid-century, because the temperature trend is reaching a threshold in which small increases in temperature are associated with exponential increases in the area burned.

Emissions from Arctic wildfires jeopardize global climate goals (*1*). The Arctic is warming rapidly because of a climate change–related phenomenon known as "Arctic amplification" (*2*); annual mean temperature has already increased more than 2°C compared with that of the preindustrial era (*3*) and is expected to reach 3.3° to 10°C above the 1985–2014 average by 2100 (*4*). These increased temperatures result in thawing of permafrost and deterioration of peatlands with emissions of carbon dioxide and methane (*5*–*7*). High-latitude peatlands are expected to become a net carbon source as a consequence of global warming (*8*). The release of carbon creates positive feedback with additional emissions contributing to further warming and thawing with further peatland degradation and emissions. In this context, the numerous fires identified by satellite thermal sensors in eastern Siberia in 2020 (*9*) raise particular concerns because of the resulting emissions (*10*).

Wildfires are common in the Arctic and Subarctic (*11*), but their size, frequency, and intensity are expected to increase as the climate warms (*12*). Extreme weather, such as that in 2020 in the Siberian Arctic (*13*), is expected to become more severe as Arctic oscillations weaken over time (*14*). Previous research in the Alaskan tundra suggests that the annual burned area might be two times greater than in the 1950–2010 period by the end of the century as warmer and drier conditions coincide more frequently (*15*). The conditions that affected the Arctic fire seasons of 2019 and 2020 in the Siberian Arctic have provided new empirical observations between climatic factors and burn extent and may already be indicating the changes in fire regimes expected by the end of the century. The fire seasons of 2019 and 2020, however, raised two uncertainties—first, whether the annual burned area above the Arctic Circle was actually increasing. Satellite-derived burned-area products tend to underestimate the true extent of burning (*12*), and rigorous validation techniques are required (*16*). Second, even if the burned areas in 2019 and 2020 were the largest yet observed, the links to other trends required evaluation.

We assessed annual burned area in the Siberian Arctic (latitudes >66.5°N) for 1982–2020 using six satellite-derived maps of burned areas (fig. S1). We investigated the Siberian Arctic because it is where most burning occurs above the Arctic Circle and fire frequency appeared to be increasing (*9*). We investigated 10 factors associated with the likelihood of fire: six climatic variables [air and surface temperature, total precipitation, wind speed and direction, and vapor-pressure deficit (VPD)], three variables describing the vegetation conditions [length of the growing season, mean normalized difference vegetation index ($NDVI_{mean}$), and climatic water deficit (CWD)], and the number of ignitions, a direct factor associated with the likelihood of fires. We evaluated how these factors have varied over the past four decades and their relationships with satellite-derived estimates of annual burned areas. Lastly, we investigated the future trends of annual burned area and fire emissions under future Representative Concentration Pathways (RCPs).

Results

Trends of burned area for 1982–2020

Between 1982 and 2020, the satellite burned-area products indicate that 12.97 million hectares (Mha) burned in the circumpolar region (latitudes >66.5°N). The Siberian Arctic, a region with continuous permafrost, accounted

[1]CREAF, Centre de Recerca Ecològica i Aplicacions Forestals, Cerdanyola del Vallès, 08193 Barcelona, Catalonia, Spain. [2]CSIC, Global Ecology Unit CREAF-CSIC-UAB, Bellaterra, 08193 Barcelona, Catalonia, Spain. [3]TheTreeMap; Bagadou Bas, 46600 Martel, France. [4]CIDE, CSIC-UV-GV, 46113 València, Spain. [5]Forest Ecology and Forest Management Group, Wageningen University and Research, Wageningen, Netherlands. [6]Center for International Forestry Research (CIFOR), Bogor 16000, Indonesia. [7]Graduate School of Agriculture, Kyoto University, Kitashirakawa Oiwake-cho, Sakyo-ku, Kyoto 606-8502, Japan.
*Corresponding author. Email: a.descals@creaf.uab.cat

ARCTIC WILDFIRES

Unprecedented fire activity above the Arctic Circle linked to rising temperatures

Adrià Descals[1,2]*, David L. A. Gaveau[3], Aleixandre Verger[1,2,4], Douglas Sheil[5,6], Daisuke Naito[6,7], Josep Peñuelas[1,2]

Arctic fires can release large amounts of carbon from permafrost peatlands. Satellite observations reveal that fires burned ~4.7 million hectares in 2019 and 2020, accounting for 44% of the total burned area in the Siberian Arctic for the entire 1982–2020 period. The summer of 2020 was the warmest in four decades, with fires burning an unprecedentedly large area of carbon-rich soils. We show that factors of fire associated with temperature have increased in recent decades and identified a near-exponential relationship between these factors and annual burned area. Large fires in the Arctic are likely to recur with climatic warming before mid-century, because the temperature trend is reaching a threshold in which small increases in temperature are associated with exponential increases in the area burned.

Emissions from Arctic wildfires jeopardize global climate goals (*1*). The Arctic is warming rapidly because of a climate change–related phenomenon known as "Arctic amplification" (*2*); annual mean temperature has already increased more than 2°C compared with that of the preindustrial era (*3*) and is expected to reach 3.3° to 10°C above the 1985–2014 average by 2100 (*4*). These increased temperatures result in thawing of permafrost and deterioration of peatlands with emissions of carbon dioxide and methane (*5*–*7*). High-latitude peatlands are expected to become a net carbon source as a consequence of global warming (*8*). The release of carbon creates positive feedback with additional emissions contributing to further warming and thawing with further peatland degradation and emissions. In this context, the numerous fires identified by satellite thermal sensors in eastern Siberia in 2020 (*9*) raise particular concerns because of the resulting emissions (*10*).

Wildfires are common in the Arctic and Subarctic (*11*), but their size, frequency, and intensity are expected to increase as the climate warms (*12*). Extreme weather, such as that in 2020 in the Siberian Arctic (*13*), is expected to become more severe as Arctic oscillations weaken over time (*14*). Previous research in the Alaskan tundra suggests that the annual burned area might be two times greater than in the 1950–2010 period by the end of the century as warmer and drier conditions coincide more frequently (*15*). The conditions that affected the Arctic fire seasons of 2019 and 2020 in the Siberian Arctic have provided new empirical observations between climatic factors and burn extent and may already be indicating the changes in fire regimes expected by the end of the century. The fire seasons of 2019 and 2020, however, raised two uncertainties—first, whether the annual burned area above the Arctic Circle was actually increasing. Satellite-derived burned-area products tend to underestimate the true extent of burning (*12*), and rigorous validation techniques are required (*16*). Second, even if the burned areas in 2019 and 2020 were the largest yet observed, the links to other trends required evaluation.

We assessed annual burned area in the Siberian Arctic (latitudes >66.5°N) for 1982–2020 using six satellite-derived maps of burned areas (fig. S1). We investigated the Siberian Arctic because it is where most burning occurs above the Arctic Circle and fire frequency appeared to be increasing (*9*). We investigated 10 factors associated with the likelihood of fire: six climatic variables [air and surface temperature, total precipitation, wind speed and direction, and vapor-pressure deficit (VPD)], three variables describing the vegetation conditions [length of the growing season, mean normalized difference vegetation index ($NDVI_{mean}$), and climatic water deficit (CWD)], and the number of ignitions, a direct factor associated with the likelihood of fires. We evaluated how these factors have varied over the past four decades and their relationships with satellite-derived estimates of annual burned areas. Lastly, we investigated the future trends of annual burned area and fire emissions under future Representative Concentration Pathways (RCPs).

Results

Trends of burned area for 1982–2020

Between 1982 and 2020, the satellite burned-area products indicate that 12.97 million hectares (Mha) burned in the circumpolar region (latitudes >66.5°N). The Siberian Arctic, a region with continuous permafrost, accounted

[1]CREAF, Centre de Recerca Ecològica i Aplicacions Forestals, Cerdanyola del Vallès, 08193 Barcelona, Catalonia, Spain. [2]CSIC, Global Ecology Unit CREAF-CSIC-UAB, Bellaterra, 08193 Barcelona, Catalonia, Spain. [3]TheTreeMap; Bagadou Bas, 46600 Martel, France. [4]CIDE, CSIC-UV-GV, 46113 València, Spain. [5]Forest Ecology and Forest Management Group, Wageningen University and Research, Wageningen, Netherlands. [6]Center for International Forestry Research (CIFOR), Bogor 16000, Indonesia. [7]Graduate School of Agriculture, Kyoto University, Kitashirakawa Oiwake-cho, Sakyo-ku, Kyoto 606-8502, Japan.
*Corresponding author. Email: a.descals@creaf.uab.cat

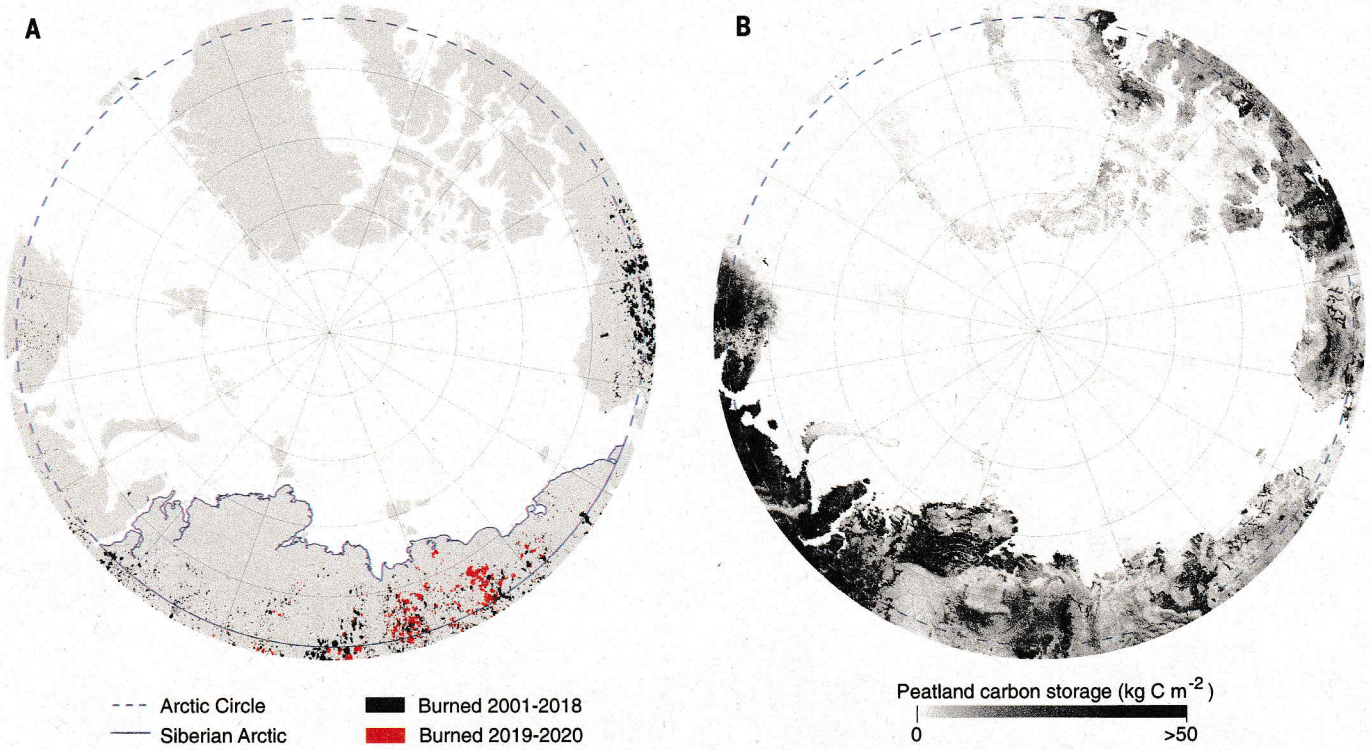

Fig. 1. Maps of burned area for 2001–2020 and peatland carbon storage in the circumpolar region. (**A**) Extent of the burns for 2001–2018 is from the FireCCI51 product, and the extent for 2019 and 2020 is the union of the C3SBA10 product and the Sentinel-2 burned-area map developed in this study. The Siberian Artic is the area inside the blue outline. Black represents areas that burned at least once for 2001–2018, and red represents areas that burned in 2019 and 2020. Areas that burned at least once in both periods, in 2001–2018 and 2019–2020, are also depicted in red; these areas represent only 3% of total burning above the Arctic Circle during the 2001–2020 period. We show the annual burned area from 2001 to 2020, which is the period when the occurrence of fires accelerated. (**B**) Estimated storage of organic carbon in peatlands from a reference dataset (*8*).

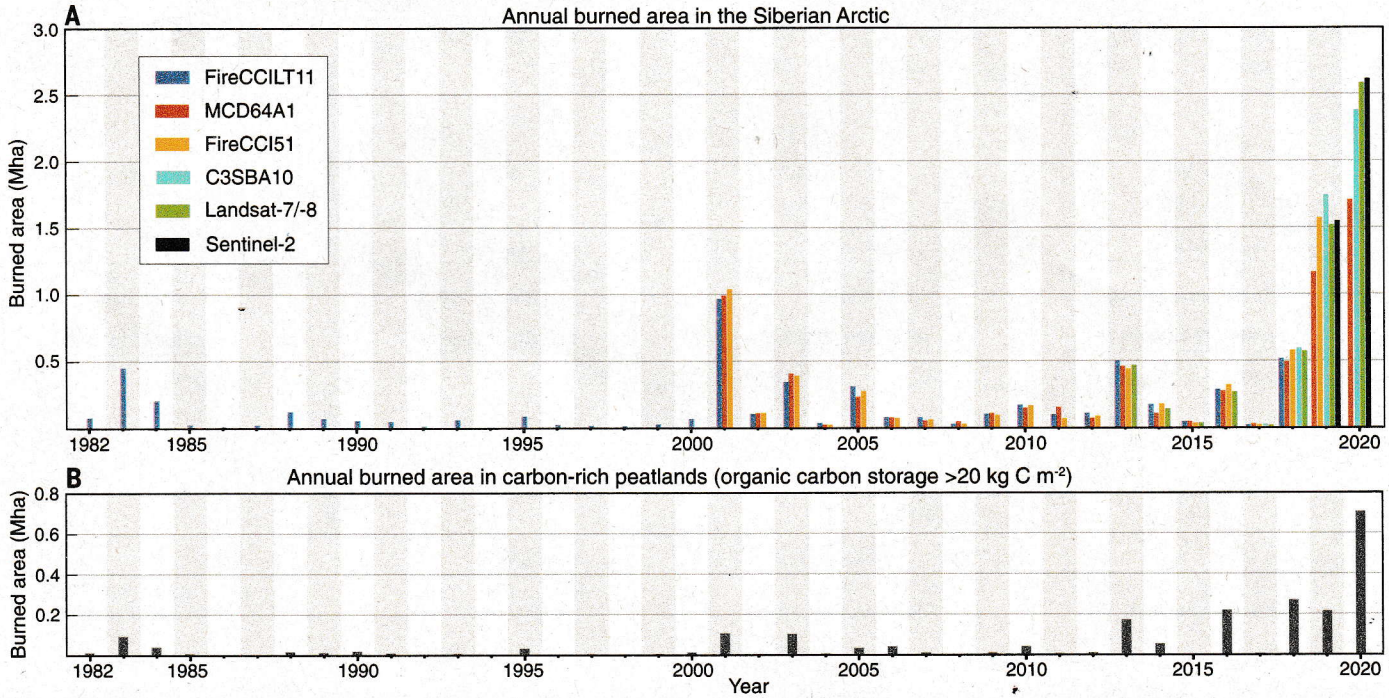

Fig. 2. Annual burned area in the Siberian Arctic and in carbon-rich peatlands for 1982–2020. (**A**) Annual burned area in the Siberian Arctic derived from remotely sensed data from six products. (**B**) Annual burned area in carbon-rich peatlands; >20 kg C m^{-2} in storage of organic carbon obtained from a reference dataset (*8*). The annual burned area in carbon-rich peatlands represents the median burned area for the available satellite products. Satellite burned-area products contain no data for 1994.

for 71% of this burned area. The years 2019 and 2020 had the greatest mapped burned area in Siberia above the Arctic Circle (Fig. 1A) (see supplementary text A for consistency of the time series of the burned area and fig. S2), which represents 44% of the total mapped burned area (9.24 Mha) in the region from 1982 to 2020. The burned area mapped in the Siberian Arctic varied between the satellite products, most notably the MCD64A1 product for 2019 and 2020 (Fig. 2A). The burned areas for 2020 were 1.71, 2.38, 2.59, and 2.62 Mha for MCD64A1, C3SBA10, Landsat, and Sentinel-2, respectively.

The sampling-based burned area in 2020, based on an assessment of errors of omission and commission (*16*), was nearly 3 Mha (MCD64A1 = 2.83 ± 0.26 Mha, C3SBA10 = 2.92 ±

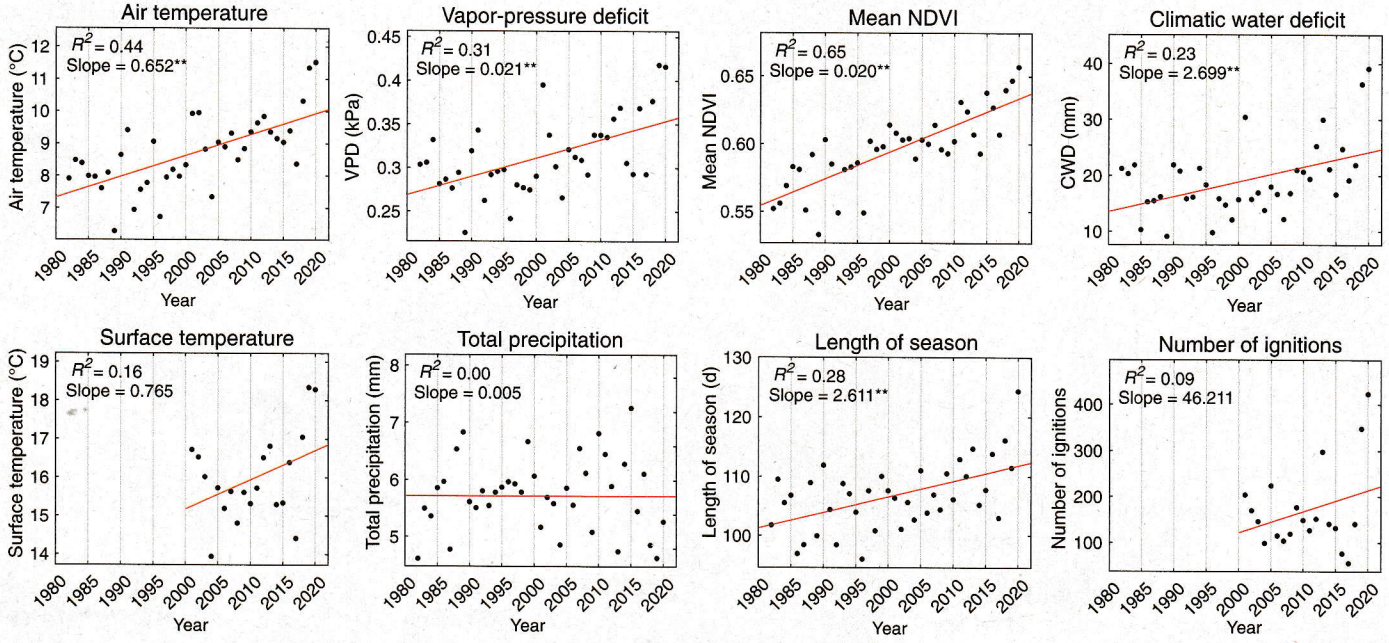

Fig. 3. Trends of eight fire factors in the Siberian Arctic during 1982–2020. Factors are the mean summer air and surface temperature, mean VPD, total summer precipitation, mean CWD, mean NDVI depicting vegetation green biomass, the length of the growing season, and the number of detected ignitions. The red lines are linear regressions; slopes are estimated on a decadal time scale. *p < 0.05; **p < 0.01.

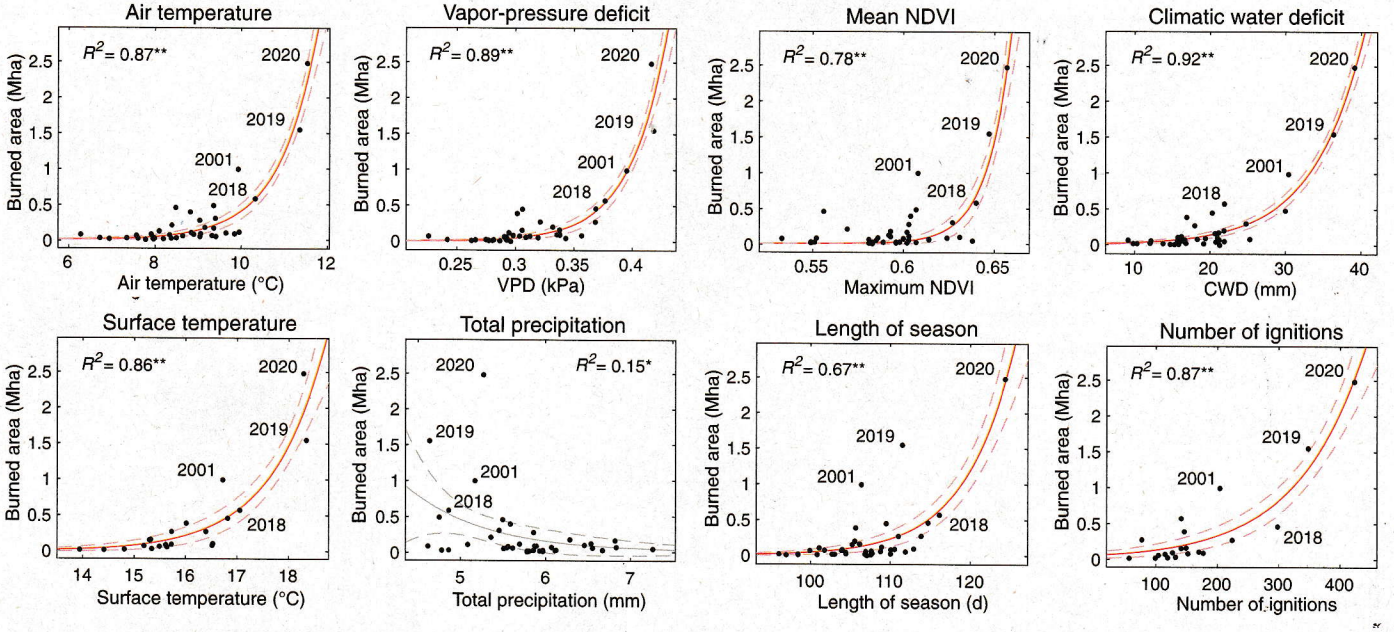

Fig. 4. Regression between the annual burned area and eight fire factors in the Siberian Arctic during 1982–2020. Solid lines are the best regression (linear or exponential), based on the coefficient of determination (R^2; *p < 0.05; **p < 0.01). The best regression model was the exponential for all the factors. The annual burned area is the median burned area for the available satellite products. The factors are the mean summer air and surface temperature, mean VPD, total precipitation, mean CWD, mean NDVI depicting green biomass, the length of the growing season, and the number of ignitions. Red solid lines depict a fit with a significant correlation (p < 0.01). The dashed lines are the 95% prediction limits of the regressions.

0.17 Mha, Landsat = 2.92 ± 0.15 Mha, and Sentinel-2 = 2.99 ± 0.14 Mha) (see full assessment of accuracy in table S1 and a description of the results in supplementary Text B). The area estimate for 2019 and 2020 amounts to ~4.7 Mha. The mapped burned area is less than the estimated burned area for all four products because the omission errors of the "burned" class (ranging from 15.5 to 53.7%) are higher than the commission errors (ranging from 3.2 to 23.0%). Our estimates of carbon emissions from burning were 55.3 and 90.4 Tg C for 2019 and 2020, respectively, which is 156.7 and 256.1 Tg CO_2-eq (including CO_2 and CH_4) (fig. S3). Fires in 2020 damaged a wide area (0.71 Mha) of carbon-rich peatlands (organic carbon storage >20 kg C m^{-2}), indicated with a reference map of soil carbon storage (Fig. 1B) (*8*). The area of carbon-rich peatlands affected by fires has also recently expanded: 70% of total burned area occurred in these areas within the past 8 years of the record, and 30% occurred in 2020 (Fig. 2B).

Trends of the fire factors for 1982–2020

Various factors that may exacerbate the risk of fire have increased significantly over the past four decades in the Siberian Arctic (Fig. 3 and fig. S4). Air temperature, NDVI, the length of the growing season, and VPD have steadily risen. The average increase in summer air temperature was 0.66°C per decade. In 2019 and 2020, the mean summer air temperature was 11.35° and 11.53°C, which was 2.65° and 2.82°C higher than the 1982–2020 average, respectively. CWD, a proxy of plant water stress defined as the difference between potential and actual evapotranspiration, also increased between 1982 and 2020, although the linear trend likely began in the 2000s. More surprising, however, was the abrupt increase in CWD in 2019 and 2020. The estimated number of ignitions, total precipitation, and wind speed all had strong interannual variations, and the slope of their trends was not significantly different from zero.

The annual number of detected ignitions was relatively consistent, with a median of 143, but high counts were observed in specific years, peaking at 423 in 2020. Seventy-two percent of these 2020 ignitions were detected within 20 days, between 13 June and 3 July, reaching Siberian Arctic regions as far north as 72.9° (fig. S5). Notably, these ignitions coincided with anomalously high values of convective available potential energy (CAPE) (fig. S6), an indicator of convective storms and lightning. Between 13 June and 3 July, satellite thermal sensors registered a rapid increase in the number of active fire detections, which accounts for 40.6% of all hot spots detected in 2020. By contrast, hot spots detected before 13 June represented only 1.1%. Similar peaks in the number of detected ignitions, preceding high rates of active fire detection, occurred concurrently with high CAPE values in 2002, 2005, 2013, and 2018.

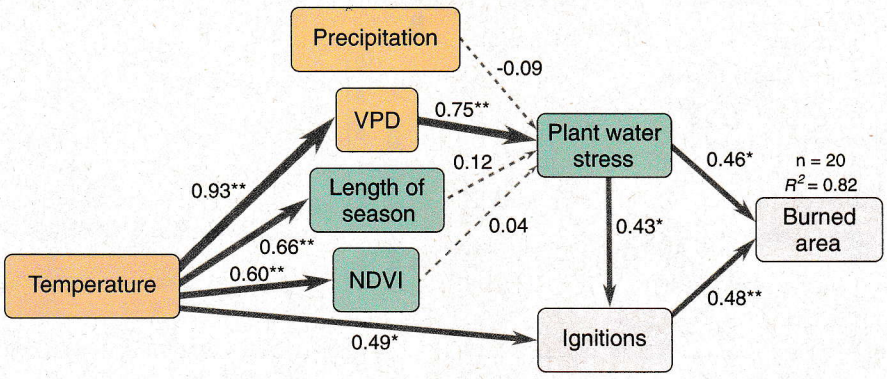

Fig. 5. Causality networks for the association among factors of fire in the Siberian Arctic for 2001–2020. Variables are categorized as climate (mean summer surface temperature, total precipitation, and mean VPD) (yellow), vegetation (mean summer NDVI depicting green biomass, the length of the growing season, and plant water stress measured by mean summer CWD) (green), and fire (number of detected ignitions and annual burned area) (light red). Factor loadings between variables are shown next to lines (*, $p < 0.05$; **$p < 0.01$). The width of the lines depicts the magnitude of the effect, and dashed lines represent nonsignificant effects. R^2 is the variance explained for the annual burned area.

Sensitivity of the burned area to the fire factors

Linear and exponential regressions were used to analyze the best association between the annual burned area (aggregated with the median across available satellites for each year) and the factors of fire regime. An exponential regression was the best regression model (Fig. 4); the annual burned area accelerated when specific thresholds were exceeded. For example, the four years with the largest mapped burned areas (2001, 2018, 2019, and 2020) had a mean summer air temperature >10°C. The best fit was for CWD, which explained 92% of the interannual variability in the burned area. Other factors with a high coefficient of determination (R^2) were summer air temperature (87%), VPD (89%), and number of ignitions (87%). The annual burned area was correlated most weakly with total precipitation (15%). We also detrended the fire factors using the linear regression shown in Fig. 3 before determining the correlation with the annual burned area to reduce the potential of spurious correlations. The detrended correlations (fig. S7) confirmed the high R^2 for CWD (90%), air temperature (80%), VPD (51%), and number of ignitions (86%), but the correlation decreased for $NDVI_{mean}$ (from 78 to 11%).

We further examined the potential relationships among the fire-related factors in a structural equation modeling (SEM) (the rationale of the proposed relationships is described in the materials and methods). The hypothesized causal model outperformed the model validity analysis ($p > 0.05$ in the chi-square test; details on the covariances and residuals in the model are shown in table S2). The SEM supported the role of temperature in controlling other factors that affect the extent of burning (Fig. 5 and fig. S8). Temperature showed significant positive relationships with the lengthening of the growing season (0.66), the vegetation green biomass represented by $NDVI_{mean}$ (0.60), and atmospheric dryness measured by VPD (0.93). We hypothesized that these temperature-regulated factors and total precipitation would influence plant water stress, measured by CWD, but only VPD showed a significant effect (0.75) for the low number of observations (n = 20). Despite this, the hypothesized relationships displayed the expected sign. Temperature and CWD had a positive relationship with the number of detected ignitions (0.49 and 0.43, respectively). Annual burned area presented an R^2 of 0.82 and was directly explained by the number of detected ignitions (0.48) and the CWD (0.46).

Climate factors may differ locally and throughout the fire season. An additional analysis based on local weather conditions during the burning revealed that ignitions affecting areas larger than 4000 ha occurred with average hourly maximum temperatures of 28.6°C (SD = 3.4°C) and mean wind direction from the northeast (fig. S9). Thirty-day preignition precipitation was 0.37 mm (SD = 0.81 mm), and mean wind speed was 0.96 m s^{-1} (SD = 0.55 m s^{-1}). Ignitions that lead to burned areas larger than 4000 ha represent only 10% of all counts but account for 81% of all burned areas that were mapped between 2001 and 2020.

Projections of annual burned area and carbon emissions under warming scenarios

Annual burned area in 2018, 2019, and 2020 more than doubled the long-term average, which was 0.24 Mha for the period 1982–2020 in the Siberian Arctic. Summer 2001, with a mean temperature nearing 10°C, was the first

occurs during relatively gentle winds blowing from the northeast, indicating that the processes that promote flammability may be distinct from those that promote the subsequent burning.

Our ignition detection method indicated that numerous fires started near simultaneously across a vast region during a period of atmospheric instability in the 2020 fire season, from which we speculate that lightning was the main cause of ignition, but local observations are required to verify this supposition. An alternative, or additional, explanation is that fires emerge from smoldering material that has persisted through the winter to reemerge when conditions permit a broader conflagration (*28*, *29*). We also found that satellite thermal sensors showed that fires spread quickly after high CAPE values and midseason ignitions, which suggests that most of the annual burned area is caused by fires that started during that time.

The link we see between fires and temperature suggests that severe fire years, such as 2020, will become increasingly common and resulting carbon emissions will rise. The magnitude of future fires and carbon emissions, however, remains uncertain. First, although the frequency of lightning strikes appears likely to increase as temperatures rise (*23*), the scale of any resulting fires depends on specific local weather and vegetation conditions, which remain challenging to predict. Second, we only considered direct emissions from burning and disregarded indirect emissions, although these are not necessarily negligible. Burning removes the peat that insulates permafrost, exposing it to thawing, which promotes soil respiration and the production of carbon dioxide and methane (*30*). Estimates from field studies in two different boreal forests in Alaska suggest that post-fire carbon emissions range from one-third to more than double those that occur during burning (*31*). Furthermore, permafrost prevents deeper burning in peatlands (*21*). As permafrost retreats, high temperatures and drying conditions may favor higher combustion rates (*32*). We used combustion rates ranging from 2.0 kg C m^{-2} for tundra to 3.4 kg C m^{-2} for boreal forests (*31*), but dry peatlands can release up to 16.8 kg C m^{-2} (*21*), indicating that much higher emissions are credible.

A previous study proposed temperature and rainfall thresholds for the annual burned areas in the Alaskan tundra (*15*). The extensive area burned in 2019 and 2020 corroborated the proposed curve-growth relationship between annual burned area and climate-related factors for the Alaskan tundra. Hu *et al.* (*15*) forecasted that the annual burned area would double in the Alaskan tundra by the end of the century. We found, however, that the annual burned area in the Siberian Arctic already doubled the long-term average in the past 3 years of the record. This increase in annual burned area suggests that the Arctic is already experiencing a change in fire regimes caused by climatic warming. The burned areas in 2019 and 2020 might be exceptional occurrences, but the recent temperature trend and projected scenarios indicate that temperatures are reaching a threshold in which small increases above 10°C can alter fire-related factors and result in exponentially increasing burned area and associated fire emissions in the next decades. Forthcoming fires can potentially affect peatlands and deteriorate the permafrost, which in turn will exacerbate the carbon emissions from carbon-rich soils.

REFERENCES AND NOTES

1. S. M. Natali *et al.*, *Proc. Natl. Acad. Sci. U.S.A.* **118**, e2100163118 (2021).
2. M. C. Serreze, J. A. Francis, *Clim. Change* **76**, 241–264 (2006).
3. E. Post *et al.*, *Sci. Adv.* **5**, eaaw9883 (2019).
4. Arctic Monitoring and Assessment Programme, *Arctic Climate Change Update 2021: Key Trends and Impacts. Summary for Policy-Makers* (Arctic Monitoring and Assessment Programme, 2021).
5. E. A. Schuur *et al.*, *Nature* **520**, 171–179 (2015).
6. K. Dutta, E. Schuur, J. Neff, S. Zimov, *Glob. Change Biol.* **12**, 2336–2351 (2006).
7. M. R. Turetsky *et al.*, *Nat. Geosci.* **13**, 138–143 (2020).
8. G. Hugelius *et al.*, *Proc. Natl. Acad. Sci. U.S.A.* **117**, 20438–20446 (2020).
9. A. Witze, *Nature* **585**, 336–337 (2020).
10. M. C. Mack *et al.*, *Nature* **475**, 489–492 (2011).
11. N. H. French *et al.*, *Int. J. Wildland Fire* **24**, 1045–1061 (2015).
12. J. L. McCarty *et al.*, *Biogeosciences* **18**, 5053–5083 (2021).
13. A. Ciavarella *et al.*, *Clim. Change* **166**, 9 (2021).
14. O. V. Churakova Sidorova, R. T. W. Siegwolf, M. V. Fonti, E. A. Vaganov, M. Saurer, *Sci. Rep.* **11**, 19010 (2021).
15. F. S. Hu *et al.*, *Front. Ecol. Environ.* **13**, 369–377 (2015).
16. P. Olofsson *et al.*, *Remote Sens. Environ.* **148**, 42–57 (2014).
17. A. Descals *et al.*, *Sci. Total Environ.* **742**, 140637 (2020).
18. L. T. Berner *et al.*, *Nat. Commun.* **11**, 4621 (2020).
19. S. Piao *et al.*, *Glob. Chang. Biol.* **25**, 1922–1940 (2019).
20. J. Peñuelas, T. Rutishauser, I. Filella, *Science* **324**, 887–888 (2009).
21. M. R. Turetsky, W. F. Donahue, B. W. Benscoter, *Nat. Commun.* **2**, 514 (2011).
22. A. B. M. Collow *et al.*, *J. Clim.* **35**, 3075–3090 (2022).
23. Y. Chen *et al.*, *Nat. Clim. Chang.* **11**, 404–410 (2021).
24. Q. You *et al.*, *Earth Sci. Rev.* **217**, 103625 (2021).
25. J. Piao, W. Chen, S. Chen, H. Gong, Q. Zhang, *J. Clim.* **33**, 3883–3899 (2020).
26. C. You, M. Tjernström, A. Devasthale, D. Steinfeld, *Geophys. Res. Lett.* **49**, e2022GL097899 (2022).
27. T. Nakamura, T. Sato, *Environ. Res.* **209**, 112881 (2022).
28. R. C. Scholten, R. Jandt, E. A. Miller, B. M. Rogers, S. Veraverbeke, *Nature* **593**, 399–404 (2021).
29. J. L. McCarty, T. E. Smith, M. R. Turetsky, *Nat. Geosci.* **13**, 658–660 (2020).
30. J. E. Holloway *et al.*, *Permafr. Periglac. Process.* **31**, 371–382 (2020).
31. S. Veraverbeke *et al.*, *Curr. Opin. Environ. Sci. Health* **23**, 100277 (2021).
32. M. R. Turetsky *et al.*, *Nat. Geosci.* **8**, 11–14 (2015).
33. A. Descals, adriadescals/ArcticFires: Arctic Fire repository, *Zenodo* (2022). https://doi.org/10.5281/zenodo.6907765.
34. E. Chuvieco, M. L. Pettinari, G. Otón, ESA Fire Climate Change Initiative, (Fire_cci): AVHRR-LTDR Burned Area Grid product, Centre for Environmental Data Analysis, Version 1.1 (2020). http://dx.doi.org/10.5285/62866635ab074e07b93f17fbf87a2c1a
35. L. Giglio, C. Justice, L. Boschetti, D. Roy, MCD64A1 MODros. Inf. Serv./Terra+ aqua burned area monthly L3 global 500m SIN grid V006, NASA EOSDIS. Inf. Serv. Land Processes DAAC (2015). https://doi.org/10.5067/MODIS/MCD64A1.006.
36. E. Chuvieco, M. Pettinari, J. Lizundia-Loiola, T. Storm, M. Padilla Parellada, ESA Fire Climate Change Initiative, (Fire_cci): MODros. Inf. Serv. Fire_cci burned area pixel product, Centre for Environmental Data Analysis, version 5.1 (2018). https://doi.org/10.5285/58f00d8814064b79a0c49662ad3af537.
37. Copernicus Climate Change Service, Fire burned area from 2001 to present derived from satellite observations, Copernicus Climate Change Service (C3S) Climate Data Store (CDS) (2019). https://doi.org/10.24381/cds.f333cf85.
38. Z. Wan, S. Hook, G. Hulley, MOD11A2 MODIS/Terra land surface temperature/emissivity 8-day L3 global 1km SIN grid V006, NASA EOSDIS Land Processes DAAC (2015). https://doi.org/10.5067/MODIS/MOD11A2.006.
39. J. Muñoz Sabater, ERA5-Land monthly averaged data from 1950 to present, Copernicus Climate Change Service (C3S) Climate Data Store (CDS) (2019). https://doi.org/10.24381/cds.68d2bb30.
40. J. T. Abatzoglou, S. Z. Dobrowski, S. A. Parks, K. C. Hegewisch, Monthly climate and climatic water balance for global terrestrial surfaces from 1958-2015, University of Idaho (2017). ttps://doi.org/10.7923/G43J3B0R.
41. H. Wouters, J. Berckmans, R. Maes, E. Vanuytrecht, K. De Ridder, Global bioclimatic indicators from 1950 to 2100 derived from climate projections, Copernicus Climate Change Service (C3S) Climate Data Store (CDS) (2021). https://doi.org/10.24381/cds.a37fecb7.
42. K. Didan, MOD13Q1 MODIS/Terra vegetation indices 16-day L3 global 250m SIN grid V006, NASA EOSDIS. Inf. Serv. Land Processes DAAC (2015). https://doi.org/10.5067/MODIS/MOD13Q1.006.

ACKNOWLEDGMENTS

Funding: This work was funded by the Ministry of Agriculture, Forestry and Fisheries (MAFF) of the government of Japan and the Center for International Forestry Research ("CIFOR"), through the project "Transitions to Climate Resilient Landscapes: Reducing and Mitigating Boreal and Tropical Forest Fires to Promote Sustainable Rural Livelihoods." We acknowledge funds from the Spanish Government grant PID2019-110521GB-I00, the Fundación Ramón Areces grant CIVP20A6621, and the Catalan Government grant SGR 2017-1005. This work represents a contribution to CSIC PTI-TELEDETECT. **Author contributions:** Conceptualization: A.D., D.L.A.G., and J.P. Methodology: A.D. and D.L.A.G. Investigation: A.D. and D.L.A.G. Visualization: A.D., D.L.A.G., and J.P. Supervision: J.P. Writing – original draft: A.D. and D.L.A.G. Writing – review and editing: A.D., D.L.A.G., A.V., D.S., D.N., and J.P. **Competing interests:** Authors declare that they have no competing interests. **Data and materials availability:** All source code and the Sentinel-2 and Landsat-8 burned-area maps are available at Zenodo (*33*). Other data that support the findings of the study are openly available. The burned area time series derived from AVHRR sensors (FireCCILT11) (*34*) is available at https://doi.org/10.5285/62866635ab074e07b93f17fbf87a2c1a. The burned area time series derived from MODIS sensors are available at https://doi.org/10.5067/MODIS/MCD64A1.006 for the MCD64A1 product (*35*) and https://doi.org/10.5285/58f00d8814064b79a0c49662ad3af537 for the FireCCI51 (*36*) product. The burned area time series derived from Sentinel-3 (C3SBA10) (*37*) is available at https://doi.org/10.24381/cds.f333cf85. The Landsat-7 and -8 surface reflectance datasets are available at https://earthexplorer.usgs.gov, and the Sentinel-2 Level-2A surface reflectance at https://scihub.copernicus.eu. The active fire datasets obtained from MODIS is available at https://firms.modaps.eosdis.nasa.gov/active_fire. Fire emission datasets were downloaded from the FIRECAM platform https://globalfires.earthengine.app/view/firecam. Land surface temperature from MODIS (MOD11A2) (*38*) is available at https://doi.org/10.5067/MODIS/MOD11A2.006. Climate reanalysis ERA5-Land Monthly (*39*) is available at https://doi.org/10.24381/cds.68d2bb30, and TERRACLIMATE dataset (*40*) is available at https://doi.org/10.7923/G43J3B0R. The downscaled air temperature projections from the HadGEM2-CC model (*41*) are available at https://doi.org/10.24381/cds.a37fecb7. The storage of organic carbon from peatlands is available at https://bolin.su.se/data/hugelius-2020. Lastly, the NDVI time series from the GIMMS3g dataset is available at https://www.nasa.gov/nex/data, and the NDVI from the MOD13Q1v6 product (*42*) at https://doi.org/10.5067/MODIS/MOD13Q1.006.

SUPPLEMENTARY MATERIALS

science.org/doi/10.1126/science.abn9768
Materials and Methods
Supplementary Text
Figs. S1 to S9
Tables S1 and S2
References (*43*–*65*)

Submitted 7 January 2022; accepted 13 September 2022
10.1126/science.abn9768